Compression Softening of Textile Cfrp Reinforced Concrete (Crc): Biaxial Testing of Cracked Crc Panels and Derivation of Constitutive Laws

Sven Bosbach *, Josef Hegger , Martin Classen

Posted Date: 13 December 2023

doi: 10.20944/preprints202312.0950.v1

Keywords: CFRP; carbon reinforced concrete; shear; compression softening; biaxial compression tension loading; cracked concrete

Article

Compression Softening of Textile CFRP Reinforced Concrete (CRC): Biaxial Testing of Cracked CRC Panels and Derivation of Constitutive Laws

Sven Bosbach *, Josef Hegger and Martin Classen

Institute of Structural Concrete, RWTH Aachen University, Aachen, Germany
* Correspondence: sbosbach@imb.rwth-aachen.de

Abstract: Due to its insensitivity to corrosion, textile CFRP (carbon fibre reinforced polymer) reinforcement enables the construction of thin-walled concrete structures such as shells, vaults and girder webs with minimal concrete cover. In contrast to tensile and flexural behaviour, strutting and compressive membrane action of cracked thin-walled carbon reinforced concrete (CRC) elements and the interaction of compressive stresses with transverse tensile loading have not yet been investigated. While for steel reinforced concrete components, extensive biaxial testing has shown a significant reduction of concrete compressive strength as a function of the lateral tensile stress (compression softening), the effect of biaxial loading on CRC structures has not been quantified yet. However, a different behaviour is expected due to different bond properties of steel and CFRP in concrete, smaller crack spacings and the tendency of the CFRP reinforced concrete for in-plane splitting. This paper presents an extensive experimental campaign for investigation of the influence of transverse tension and cracking on the compressive strength of CRC with refined measurement techniques. Based on a literature review on compressive softening behaviour and conventional test setups for steel reinforced concrete, a novel test setup was developed. The phenomenology of compression softening in CRC as well as the main factors influencing compressive membrane behaviour are highlighted. Based on the experimental findings a constitutive law for compression softening behaviour of CRC is proposed.

Keywords: CFRP; carbon reinforced concrete; shear; compression softening; biaxial compression tension loading; cracked concrete

1. Introduction

Carbon reinforced concrete (CRC) structures with textile carbon fibre reinforced polymer (CFRP) reinforcement are characterised by high compressive and tensile strengths and have great potential for use in thin-walled structures such as shells or webs of beams that are predominantly subjected to in-plane compressive forces (e.g., [1–10]). As a result, lightweight, high-performance and durable structures can be designed with a minimum of material use for sustainable structures [11]. For such structures, an adequate prediction of the capacity of concrete struts is of crucial importance. In particular, specimens with thin webs, high shear reinforcement ratios or with flat stress field angles are prone to strut failure. Understanding the structural behaviour of CRC under combined compressive and transverse tensile loading is essential as a reduction of strength compared to the uniaxial compressive strength is likely to occur. For steel reinforced concrete structures, extensive research using panel tests on reinforced concrete specimens has shown a significant reduction of the concrete compressive strength as a function of the lateral tensile stress of up to half of the uniaxial compressive strength. In contrast to steel reinforced concrete, the stress transfer mechanisms in CRC under multi-axial loading are largely unexplored yet. Due to the different bond properties of the textile CFRP reinforcement compared to steel reinforcement, the reduced crack spacing and the tendency of the concrete for in-plane splitting, a different behaviour under biaxial loading is expected compared to steel reinforced concrete. Therefore, the experimental investigation of the capacity of the compression strut is essential. As the influences of transverse tension and cracking have not been investigated in detail, systematic test series using a new test setup and refined measurement

 doi:10.20944/preprints202312.0950.v1

techniques were carried out. Based on the experimental findings a constitutive law for description of the compressive strength of CRC compared to plain HSC taking into account the influence of transverse tension is presented in this paper.

2. Compressive strength of CRC

The compressive capacity of plain high strength concrete (HSC), commonly used for CRC, under biaxial loading is highly dependent on the transverse load applied. While the reduction of strength for biaxial compression-tension of HSC is even more pronounced than for normal strength concrete (e.g., [12]), biaxial compression loading results in an increased load-bearing capacity [13]. The presence of textile CFRP reinforcement embedded in HSC matrix, which is sensitive to lateral pressure [14], reduces the compressive strength of CRC. For non-impregnated textile reinforcement, the yarns are therefore usually considered as voids that weaken the concrete cross-section [15,16]. Both the weft and warp direction of typical biaxial grids form artificial discontinuities [17]. However, this type of disturbance becomes more pronounced as the number of layers increases and the thickness of the concrete between the yarns decreases [18], eventually leading to a separation and splitting of the CRC panel along the CFRP grids into several thin concrete lamellae. This separation can lead to premature failure of the concrete lamella due to second order deformations as their effective thickness is reduced. For CRC with impregnated yarns, extensive research has been carried out by BOCHMANN to investigate the behaviour under uniaxial compression [18,19]. He investigated the phenomenon of the reduction of compressive strength for textile reinforced cubic CRC specimens (40 mm edge length) with different reinforcement inclinations in relation to the direction of compressive forces and different manufacturing methods, as well as impregnation materials of the reinforcement (styrene-butadiene (SBR) and epoxy resin (EP), respectively). BOCHMANN proposed a reduction of compressive strength as a function of the reinforcement ratio and the inclination of the stress field to the plane of the reinforcement. In his tests, he found that EP-impregnated grids have a significantly smaller reduction of compressive strength than SBR-impregnated grids due to the higher transverse stiffness of the resin [20]. In addition, a significant influence of the fabrication method has been observed. The reduction is more pronounced for specimens that have been produced by lamination [21] in comparison to cast specimens due to the interlaminar joint in the reinforcement plane resulting in premature failure. Similar results were found by BIELAK in [22] for CRC cubes with EP impregnated grids. According to MOCCIA ET AL. [23], the casting position also affects the compressive strength of reinforced concrete due to voids under the reinforcement bars resulting from bleeding and plastic settlement of the fresh concrete. For example, for webs in thin CRC girders, these voids may occur below the longitudinal yarns for example in flanges in tension and compression zones. In addition, the formation of voids is dependent on the concrete slump and compaction quality of the concrete.

For CRC specimens, biaxial compression tests with soft-impregnated CFRP grids and HSC with a maximum aggregate size of 1 mm were recently performed by BETZ [24]. These tests showed a reduction of compressive strength for a lateral pressure that was greater than 50% of the uniaxial prismatic compressive strength. No significant reduction of compressive strength was observed at lower lateral pressures. The utilized grids act as a cross-sectional weakening, causing the specimens to fail prematurely by splitting in the reinforcement plane. For higher reinforcement ratios and laminated specimens, this effect was more pronounced. It was also found that higher reinforcement ratios resulted in lower compressive stiffness of the CRC specimens.

As in steel reinforced concrete, the capacity of compression struts in CRC cannot be described solely by the uniaxial or biaxial compressive strength, since additional transverse tensile stresses are induced, for example, by the longitudinal and transverse yarns of CFRP shear reinforcement in webs of slender beams (Figure 1 (a)). In particular, thin-walled CRC components reinforced with CFRP grids are prone to strut failure due to their thin webs, high shear reinforcement ratios and flat stress field angles. In highly reinforced webs of CRC components, compression strut inclinations of 45° occur, while the yarns are oriented horizontally and vertically. Both the longitudinal and the vertical yarns induce tensile stresses in the compression strut due to bending and shear. These transverse

Preprints (www.preprints.org) | NOT PEER-REVIEWED | Posted: 13 December 2023 doi:10.20944/preprints202312.0950.v1

tensile stresses (and thus strains) reduce the compressive strength and stiffness in cracked CRC. This behaviour is well known for steel reinforced concrete and is referred to as compression softening (Figure 1 (b)). These stress states can be represented in a simplified form in 2D with a CRC specimen subjected to compressive stresses and transverse tension (0°/90° orientation). In addition, the 45° inclination of the reinforcement relative to the compression strut must also be considered in experimental investigations. It is important that both the warp and the weft yarns are subjected to tensile forces (Figure 1 (a).

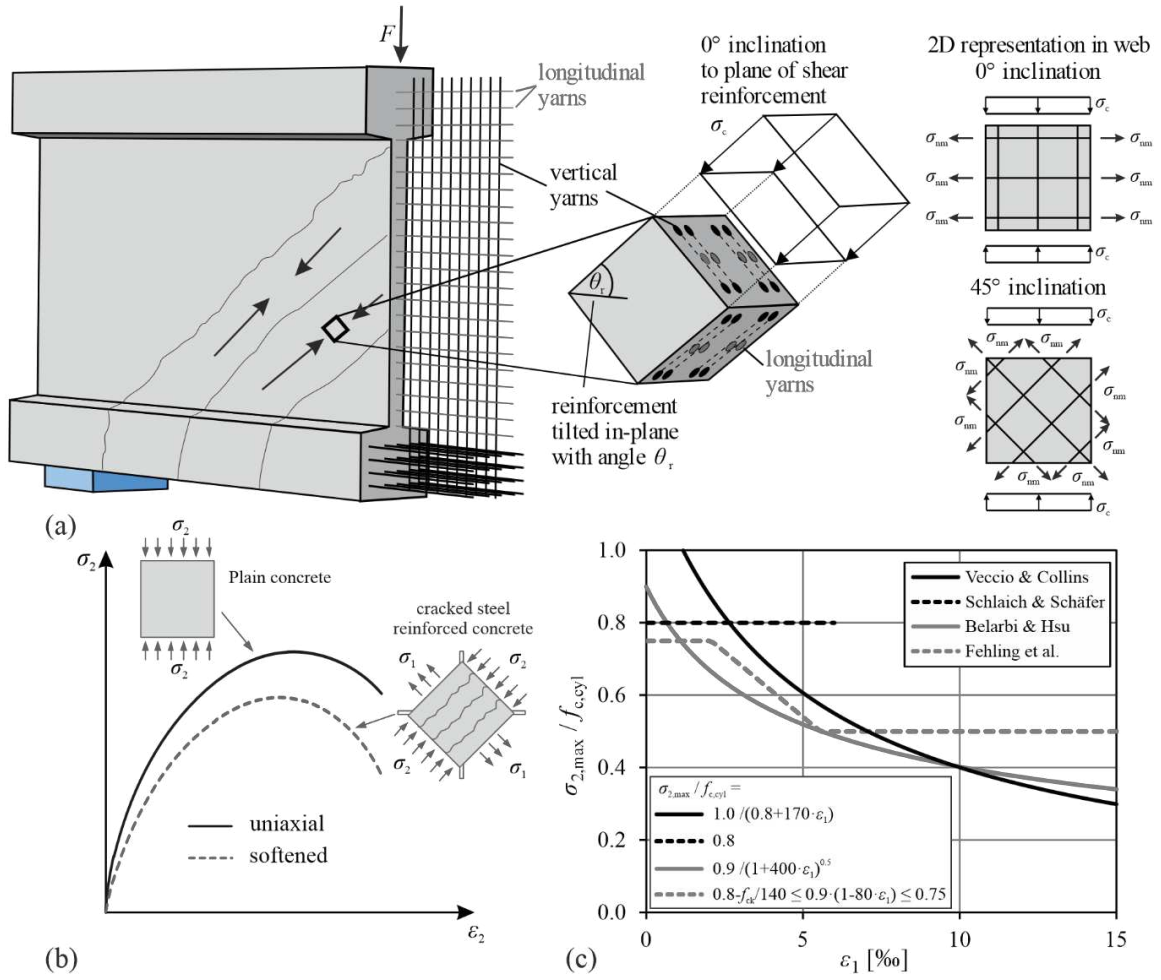

Figure 1. Orientations of uniaxial compression stresses to reinforcement in a CRC web [17] (a), compression softening of steel reinforced concrete following [25] (b) and exemplary constitutive laws for compression softening in steel reinforced concrete. (c)

In general, two different test setups have been used by researchers in the past to investigate compression softening in steel reinforced concrete: panel tests (e.g. [26–29]) and biaxial compression – transverse tension tests on reinforced panels (e.g., [30–34]). In these tests, for example panels were loaded in compression in one direction while transvers tension was applied, and also different load controls were used (e.g., proportional / sequential loading). Further information can be found in [35]. The constitutive laws proposed by the researchers to account for compression softening in steel reinforced concrete based on their experimental investigation vary strongly (Figure 1 (c)). While SCHLAICH & SCHÄFER [34] proposed a constant reduction of strength to 80% of the cylindrical compressive strength $f_{c,cyl}$ for average transverse tensile strains ε_1 of the reinforced concrete panels up to 6‰ (no experimental results are available for higher strains), VECCIO & COLLINGS [29] and BELARBI & HSU [26] suggest exponential reductions as a function of the average tensile strain ε_1. In [31] a trilinear law is proposed instead. Here, a reduction to $0.75 \cdot f_{c,cyl}$ is chosen for average tensile strains ε_1 up to 2 ‰ and $0.5 \cdot f_{c,cyl}$ (for f_{ck} = 40 MPa) for yielding of steel with average strains ε_1 higher than 6

‰, with linear interpolation in between. In the new generation of Eurocode 2 [36] the influence of the average longitudinal tensile strain in mid-depth of the stress-field ε_x as well as the inclination of compression strut θ_r is included in the reduction of the compressive capacity of steel reinforced concrete.

Such extensive experimental investigations considering the influence of transverse tension on the compressive strength have not yet been carried out for components with non-metallic reinforcement. In tests on textile reinforced concrete (TRC) panels with non-impregnated alkali resistant glass fibres in [16,37] it was found that a simple transfer of the panel-testing method is challenging for thin-walled TRC because of stability problems and issues with the load introduction. However, tests have also been carried out in a panel tester for steel reinforced concrete components strengthened with FRP sheets [38]. In these studies, the results of [26] were confirmed, but with reduced softening behaviour due to the applied FRP sheets. VOSS proposed a large reduction of compression strut capacity of 29,7 % for non-impregnated textile reinforcement [16], which was recalculated based on the results of his flexural shear tests with strut failure. For specimens with impregnated textile reinforcement, the influence of transverse tension on the compressive strength has not been systematically investigated yet. The higher ultimate strains and stresses in the CFRP reinforcement may result in higher tensile stresses in the surrounding concrete compared to steel reinforcement. In addition, longitudinal cracks resulting from bond stresses of the reinforcement could split the compression struts and induce spalling of the concrete [17]. BIELAK ET AL. found in large-scale bending tests on CRC I-beams with textile CFRP shear reinforcement that the capacity of the compression strut is further reduced compared to steel reinforced concrete [39]. In his specimens, four layers of epoxy impregnated CFRP grids were assembled into the 5 cm thick web. The significantly reduced concrete cover and high shear reinforcement ratio caused premature bond failure and in-plane cracking. Recently, first tests on the biaxial compression-tension behaviour of CRC based on BOCHMANN's investigation of the uniaxial compressive behaviour of CRC [18]were conducted by BETZ ET AL. [40]. They used fine-grained concrete with a maximum aggregate size of 1 mm and soft impregnated grids, which resulted in a relevant reduction in compressive strength up to 40 % for casted panels in dependence on the maximum tensile strain in the yarns of up to approximately 7 ‰. In addition, they found the well-known influence of the fabrication method with further reduction in strength of laminated specimens. However, a systematic experimental campaign to quantify the effect of compression softening of CRC is not yet available.

3. Experimental Investigation

3.1. Materials

3.1.1. Concrete

For a systematic investigation of the compression softening behaviour in CRC, uniaxial compression and biaxial compression-tension test were performed. Therefore, a high-strength, self-compacting concrete (C3-HF2-165-4) with a maximum aggregate size D_{max} of 4 mm was used for all specimens, which is an adaption of the concrete from [41] and has also been used, for example in [42], [43]. The concrete mixture is given in Table 1. After concreting, the test specimens were left in the formwork for one day and then wrapped in moist jute fabric for seven days to prevent cracking due to shrinkage. They were then stored at 20°C and 65 % RH until the day of testing. The compressive strength of cubes (150 × 150 × 150 mm³) and cylinders (d/h = 150/300 mm) according to [44] and the Young's modulus according to [45] were determined on the day of testing. In addition, the compressive strength and flexural tensile strength were determined on prisms (40 × 40 × 160 mm³) according to [46]. The properties of the concrete on the day of testing are given in section 4.

Preprints (www.preprints.org) | NOT PEER-REVIEWED | Posted: 13 December 2023 doi:10.20944/preprints202312.0950.v1

Table 1. Composition of used concrete.

Ingredient		Density [kg/m³]	Content [kg/m³]	Ratio [%]
Cementitious binder compound BMC CEM II/C-M Deuna		2962	707	29,9
Water		1000	165	7,0
Fine quartz sand	F38 S	2650	294	12,4
Quartz sand	0.1–0.5 mm	2650	243.2	10,3
Quartz sand	0.5–1.0 mm	2650	201.4	8,5
Quartz sand	1.0–2.0 mm	2650	148.9	6,3
Quartz fine gravel	2.0–4.0 mm	2650	593.5	25,1
Superplasticizer MC-VP-16–0205-02		1070	15	0,5

3.1.2. Textile CFRP reinforcement

All specimens were made using a symmetric biaxial planar epoxy impregnated CFRP grid with a yarn spacing of 38 mm in both directions. Tensile tests according to [47] were performed on the yarns in warp and weft directions to characterise the tensile strength and the Young's modulus [48]. Table 2 shows the mean values obtained from $n = 3$ tests each. For the tests carried out on the CRC panels, the weft yarns were oriented perpendicular to compression load. Although the Young's moduli were in a similar range, the tests with preformed grids with yarns inclined at 45° to the direction of the compression strut showed a significantly lower tensile strength than the tests with planar grids [49].

Table 2. Material properties of textile CFRP reinforcement [48,49]

Type of reinforcement	Material	Cross section* [mm²/m]		Distance between roving axes [mm]		Tensile strength [MPa]		Young's Modulus [GPa]	
		0°	90°	0°	90°	0°	90°	0°	90°
Planar grid	CFRP	95	95	38	38	3710	3490	231	244
Preformed grid	CFRP	95	95	38	38	2600	1930	219	191

* pure fiber cross-section without resin.

In addition, uniaxial tensile tests were performed on CRC specimens with two and three layers of the planar CFRP grid according to [50] and [47] to investigate the delamination and crack development in highly reinforced CRC specimens using digital image correlation (DIC) and linear variable differential transformers (LVDTs). The test setup and specimen geometry are shown in Figure 2 (a). Figure 2 (b) shows the stress-strain diagrams of the specimens measured with LVDTs. The three well-known crack stages I, IIa and IIb according [50] were observed for all specimens. Due to limitations in the maximum capacity of the test setup, the three-grid specimens could not be loaded up to yarn failure (premature slip in the clamping). However, these specimens showed no delamination failure up to a mean tensile strain of 2700 MPa. It can therefore be concluded that the original objective of analysing the delamination and crack stages was achieved in all tests. The specimen reinforced with two grids had a premature delamination failure reaching an average of 90 % of the yarn tensile strength according to Table 2. The crack evolution was evaluated in detail using the DIC evaluation. Cracking starts at a mean tensile strain of 0.7 ‰, while the crack pattern is completed at strains of 5.3 ‰ (2 grids) and 4.7 ‰ (3 grids), respectively (Figure 2 (d)).

Preprints (www.preprints.org) | NOT PEER-REVIEWED | Posted: 13 December 2023 doi:10.20944/preprints202312.0950.v1

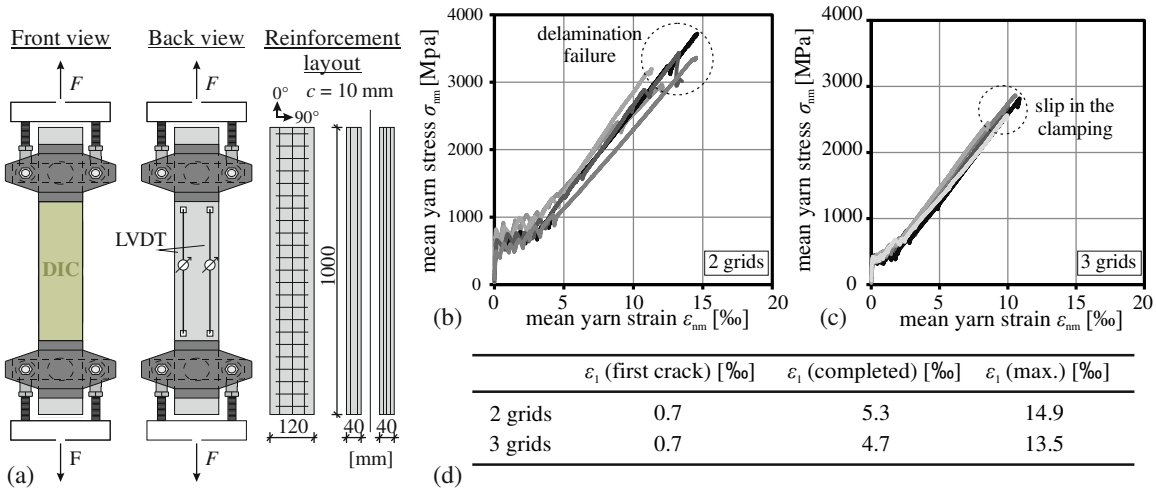

(d)

	ε_1 (first crack) [‰]	ε_1 (completed) [‰]	ε_1 (max.) [‰]
2 grids	0.7	5.3	14.9
3 grids	0.7	4.7	13.5

Figure 2. Uniaxial tensile test on CRC specimens reinforced with two and three grids: test setup and geometry (a), stress-strain diagrams of specimens with two grids (b) and three grids (c) and measured strains at different crack stages using DIC evaluation (d).

3.2. Test setup and procedure

To investigate the compression softening behaviour of slender CRC panels (height h / thickness $t > 2$), a novel combined compression – transverse tension test setup was developed following the test setups of e.g., [32,34,51], (Figure 3 (a)). The use of conventional panel tests as in [29] or [26], cannot be simply adopted for carbon reinforced concrete due to premature stability failure, as shown in investigations in [16,37].

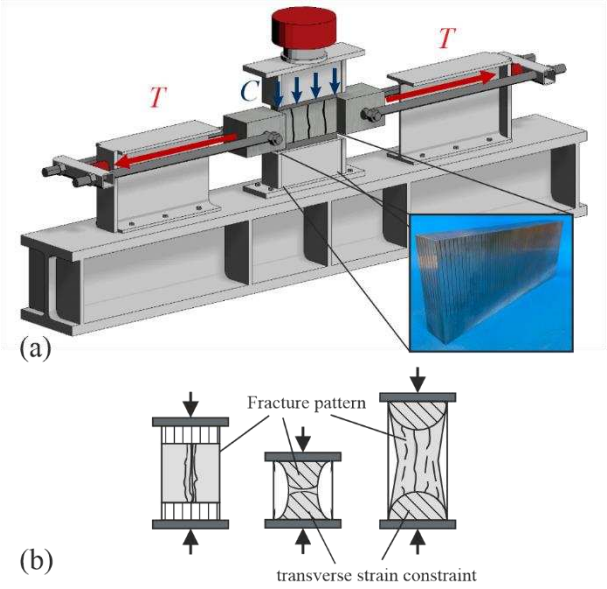

Figure 3. Test setup for investigation of compression softening (a) and influence of different load application systems (b).

For the application of tensile forces, a stiff frame was installed whereby the normal force is introduced from both sides into the centre of the specimen via steel bolts, similar to the test setup in [17,52], so that the centre of the specimens remains located centrally under the compression force application. Thus, the reinforcement does not need to be clamped and lateral pressure can be avoided. The test specimens were segmented into a central part, containing the test area, and two outer parts for inducing axial tension. The three parts are only connected by reinforcement and the concrete separated by PE sheets to prevent the transfer of compressive stresses between these areas (Figure 4).

 doi:10.20944/preprints202312.0950.v1

Vertical and axial loads are controlled by two different hydraulic cylinders, allowing various combinations of tension (T) and compression (C) loads to be applied. For the application of compression, brush bearing platens were used in accordance to [13,53], in order to minimize the transverse constraint that unavoidably occurs through friction when using rigid steel plates as load application [54] (Figure 3 (b)). A conical/spherical steel bearing was placed on the frame of the upper brush bearing platens to reduce the influence of eccentricities [18]. In addition, the top and bottom sides of the test specimens were face-milled prior to testing to achieve an ideal flat surface for uniform application of compressive load. An accuracy of ≤ 2.5 ‰ measured with a sliding calliper was realized, thus meeting the requirements of [55].

Test specimens

For the biaxial tests, small panels with two and three layers of textile CFRP reinforcement and a distance between the reinforcement centroid and the specimen edge of d_1 = 10 mm and d_1 = 15 mm, respectively, were selected. Smaller concrete covers are not suitable for investigation, as bond requirements for tensile loads must be met. The dimensions of the specimens that were exposed to biaxial loading (compression and transverse tension) were 300 × 40 × 145 mm³. The length was chosen to allow for evolution of multiple cracks due to the transverse tensile force in the loaded region of the specimen while keeping the dimensions as small as possible. Both anchorage parts had a thicker cross section (140 × 145 mm²) and additional reinforcement layers to prevent premature failure in these areas. Reference tests with two to four grids were carried out with the dimensions of the test area in the biaxial tests (Figure 4 (a)). While four grid layers were tested in the uniaxial compression tests, a maximum of three layers were examined in the biaxial tests, as higher reinforcement ratios would already lead to premature splitting failure in uniaxial tension due to excessive bond stresses. As described in section 2, the stress states occurring in compression struts can be represented simplified in 2D with CRC specimens subjected to compression stresses and transverse tension (0°/90° orientation), but 45° inclined reinforcement also needs to be tested where both the warp and the weft yarns are subjected to tensile stresses simultaneously. Therefore, two different cross sections were required for biaxial compression-tension testing (θ_r = 0° in Figure 4 (b) & θ_r = 45° in (c)). For the tests with skewed yarns, preformed textile grids were used since they offer sufficient anchorage of the yarns [56].

Preprints (www.preprints.org) | NOT PEER-REVIEWED | Posted: 13 December 2023 doi:10.20944/preprints202312.0950.v1

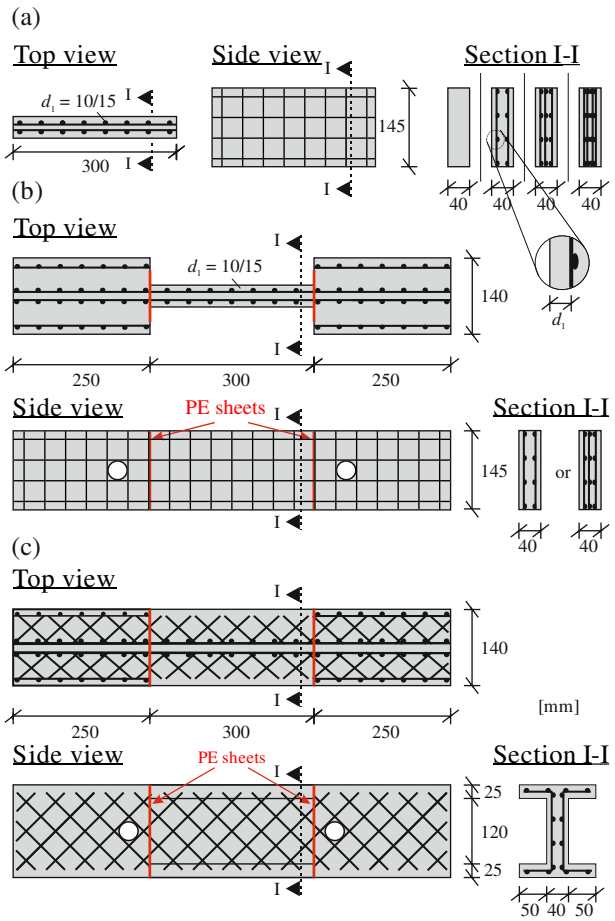

Figure 4. Specimen dimensions and reinforcement layout of uniaxial compression tests (a) and biaxial compression-tension tests (b) and (c).

Test series

In total, 50 specimens were tested, 22 specimens with uniaxial compression and 28 specimens with biaxial loading. Within the uniaxial compression tests the influence of the specimen dimensions and the brush bearing platens, as well as the influence of CFRP reinforcement ratio and concrete cover on the uniaxial compressive behaviour was investigated. In the tests with biaxial loading the sequence of load application (sequential / proportional), the concrete cover, the reinforcement ratio, the inclination of reinforcement and the maximum average tensile strains of the CRC specimens were varied. While the compressive forces were applied strain-controlled with a constant ratio of 2 µm/s following [18], the tensile forces were applied force-controlled with varying ratios to achieve different maximum tensile strains at compression failure of the specimens. An overview of the test series carried out and the parameters varied is given in Table 3.

Table 3. Main parameters of test series.

Test series	# of tests	type of loading	d_1 [mm]	ρ [%]	grid orientation [mm]	investigated influence
CS-1	3	uniaxial compression	plain concrete			panel geometry
CS-2	3	uniaxial compression via steel platens	plain concrete			load introduction
CS-3	3	uniaxial compression	10	0.5	0°/90°	presence of grids
CS-4	5	uniaxial compression	15	0.5	0°/90°	concrete cover
CS-5	3	uniaxial compression	10	0.75	0°/90°	reinforcement ratio

Preprints (www.preprints.org) | NOT PEER-REVIEWED | Posted: 13 December 2023 doi:10.20944/preprints202312.0950.v1

CS-6	3	uniaxial compression	10	1.00	0°/90°	reinforcement ratio
CS-7	6	biaxial proportional	10	0.5	0°/90°	$\sigma_{nm1} / \sigma_{c2}$ = 3.9 … 44.9
CS-8	6	biaxial proportional	15	0.5	0°/90°	$\sigma_{nm1} / \sigma_{c2}$ = 3.9 … 38.7
CS-9	6	biaxial proportional	10	0.75	0°/90°	$\sigma_{nm1} / \sigma_{c2}$ = 4 … 36.7
CS-10	3	biaxial sequential	10	0.5	0°/90°	$\sigma_{nm1,seq}$ = 901 … 2345 MPa
CS-11	4	biaxial proportional	10	0.5	0°/90° preformed	$\sigma_{nm1} / \sigma_{c2}$ = 14.7 … 38.4
CS-12	3	biaxial proportional	10	0.5	45°/45° preformed	$\sigma_{nm1} / \sigma_{c2}$ = 14.5 … 27.9

d_1: distance between reinforcement centroid and specimen edge, see Figure 4; ρ: geometrical reinforcement ratio; $\sigma_{1,seq}$: yarn stress at beginning of compression loading; $\sigma_{nm1} / \sigma_{c2}$: ratio of axial yarn stress ($\sigma_{1,nm}$) to transverse concrete compressive stress ($\sigma_{2,c}$).

3.3. Instrumentation

In all tests, the deformations were measured in the test area using DIC from one side and conventional vertical and horizontal LVDTs attached to the opposite side of the specimen. Horizontal deformations are measured using two LVDTs, while vertical deformation was measured using three distributed LVDTs. In addition, fibre optic sensors (FOS) were attached to all horizontal yarns in the test area of the biaxial tests with cyanoacrylate adhesive according to [57,58] to measure the yarn strain continuously according to [59]. The locations of the LVDTs, DIC and FOS are shown in Figure 5.

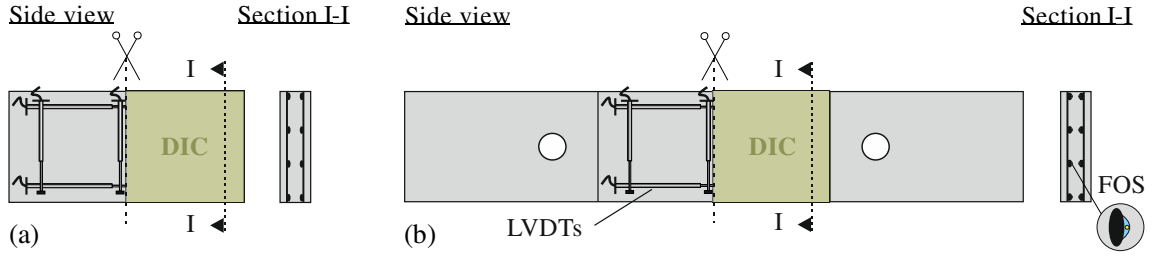

Figure 5. Instrumentation for uniaxial compression tests (a) and for biaxial tests (b): LVDTs on back side, DIC on front side of specimens and FOS on longitudinal yarns under investigation (in biaxial tests).

4. Results and discussion

4.1. Uniaxial compressive tests

In contrast to the tests in [18], slender panels (h/t = 3.6) were investigated, which might exhibit a different behaviour compared to the small cubes investigated by BOCHMANN. Therefore, in a first step, the uniaxial compressive strength of plain concrete $\sigma_{c2,max}$ was determined and compared to the compressive strength $f_{c,cyl}$ determined with cylinders (d/h = 150/300 mm) according to [44], whose strength is usually used for design in Europe [60]. In addition, the influence of the load application system was investigated with a test series using conventional steel platens for compressive loading. Afterwards, the influence of the concrete cover and the CFRP grids on the compressive strength of the panels was studied. The average results of uniaxial compression tests (3-5 tests each) are summarised in Table 4. The compressive strength here is calculated using the exact dimensions measured with sliding gauge and neglecting the cross-section of yarns.

Preprints (www.preprints.org) | NOT PEER-REVIEWED | Posted: 13 December 2023 doi:10.20944/preprints202312.0950.v1

Table 4. Test results of uniaxial compression tests.

Test series	d_1 [mm]	ρ [%]	$f_{c,cyl}$ [MPa]	$\sigma_{c2,max}$[1] [MPa]	$\sigma_{c2,max} / f_{c,cyl}$ [-]
CS-1	-	-	92.7	93.3	1.01
CS-2	-	-	92.7	85.7	0.92
CS-3	10	0.5	92.7	79.8	0.86
CS-4	15	0.5	96.2	85.4	0.89
CS-5	10	0.75	96.4	92.0	0.95
CS-6	10	1.00	96.2	83.0	0.86

[1]calculated using the exact dimensions of gross cross section measured with sliding gauge.

Figure 6 (a) shows the uniaxial compressive strengths determined in the test series CS-1 -3. All specimens were produced on the same day and tested after a sufficient time of hardening of at least 40 days. The panel strength determined with steel platens (CS-1) is identical to the cylindrical compressive strength. The use of the brush bearing platens provides a lower compressive strength (CS-2). As illustrated in Figure 6 (b), the fracture patterns of plain concrete specimens (CS-1 and 2) are also significantly different for the specimens loaded by steel platens (top) and brush bearing platens (centre) due to the flexibility of the small steel brushes and the resulting reduced lateral restraint which allows individual uniform concrete lamellae to form due to unconfined uniaxial loading.

For the specimens with two layers of CFRP grids with d_1 = 10 mm loaded with brush bearing platens, a further reduction of strength can be observed due to the embedded CFRP yarns that cause a deviation of compressive stress flow. Due to their smaller Young's modulus the CFRP grids act as a cross-sectional weakening, causing the specimens to fail prematurely by splitting in the reinforcement plane. The failure of these specimens is therefore characterised by delamination of the concrete cover as shown in Figure 6 (b) (bottom). The formation of individual lamellae is largely prevented by the grids.

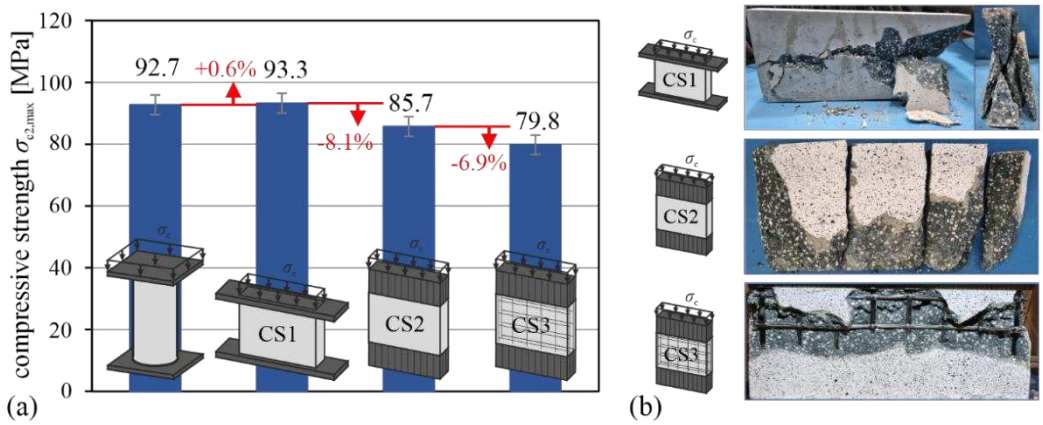

Figure 6. Influence of specimen geometry and CFRP grid on the uniaxial compressive strength (a) fracture patterns of investigated specimens (b).

Furthermore, an additional series of tests (CS-4, CS-5, CS-6) with different configurations of CFRP grids compared to the reinforced reference test CS-3 has been carried out to further analyse the influence of textile reinforcement on uniaxial compressive behaviour.

In these tests, two effects have been observed, which are partly counteracting each other (Figure 7): On the one hand, adding more CFRP grids potentially increases the number of potential locations where vertical splitting cracks may be induced due to stress deviations (effect ①). On the other hand, adding additional CFRP grids (increasing the reinforcement ratio) leads to an increased (passive) confinement in longitudinal direction of the panel (effect ②) which can have a beneficial effect on concrete strength.

Effect ① can be well isolated by testing specimens with identical concrete dimensions and reinforcement ratios but different number of layers that cause the deviation of concrete stresses. In

Preprints (www.preprints.org) | NOT PEER-REVIEWED | Posted: 13 December 2023 doi:10.20944/preprints202312.0950.v1

test series CS-3 the position of the CFRP grids (concrete cover d_1 = 10 mm) caused stress deviations in two layers, while in CS-4 the two grids where concentrated in the middle of the panel (concrete cover d_1 = 15 mm). In consequence, in CS-4 the deviation of compressive stresses occurred only around a single weak layer in the middle of the panel, while larger stress redistributions around two reinforcement layers occurred in CS-3. Thus, a higher resistance was found in CS-4.

On the other hand, adding additional CFRP grids (increasing the reinforcement ratio) leads to an increased confinement in longitudinal direction of the panel (effect ②). The interaction of both effects ① and ② can be observed when comparing the results of series CS-3 with series CS-5 and CS-6. In CS-5 and CS-6 the beneficial effect ② of higher confinement in longitudinal direction compensates the reduced net concrete area and larger stress deviations due to additional CFRP grid layers. Eventually, none of the tested configurations in CS-4, CS-5, CS-6 showed any further reduction in compressive strength compared to the reinforced reference tests (series CS-3).

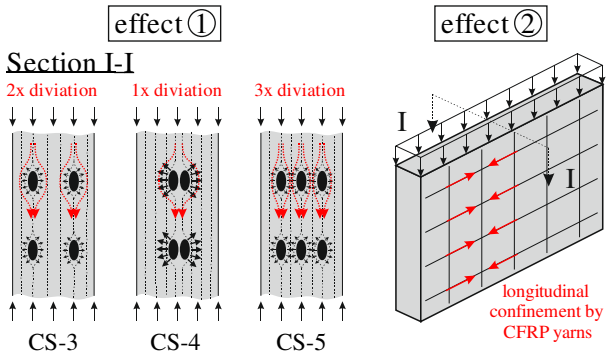

Figure 7. Occurring effects of CRC panels under uniaxial compression: Splitting tensile stresses resulting from deviation of compression stresses due to yarns (effect ①) and confinement due to CFRP grids (effect ②).

4.2. Biaxial compression-tension tests

4.2.1. Phenomenology

Influence of transverse tension on compressive strength

Figure 8 (a) shows the ratio of the compressive strength of panels $\sigma_{c2,max}$ and the compressive strength of cylinders $f_{c,cyl}$ for the transverse tensile strain ε_1 acting at compressive failure for all biaxial tests performed. The identical symbols are associated to the uniaxial and biaxial tests with the same configuration (d_1 / ρ / grid orientation). In general, a significant reduction of compressive strength was found for increased average transverse tensile strains, analogously to steel reinforced concrete. As expected, more cracks were found at higher tensile strains. The maximum tensile strain $\varepsilon_{1,max}$ in all diagrams corresponds to the average panel strains evaluated by DIC. For steel reinforced concrete, the biaxial compressive strength is significantly influenced by the crack width and the crack spacing [34,51,61,62]. Due to the close-meshed CFRP grid, smaller crack spacings and smaller crack widths occur in the CRC specimens.

Preprints (www.preprints.org) | NOT PEER-REVIEWED | Posted: 13 December 2023 doi:10.20944/preprints202312.0950.v1

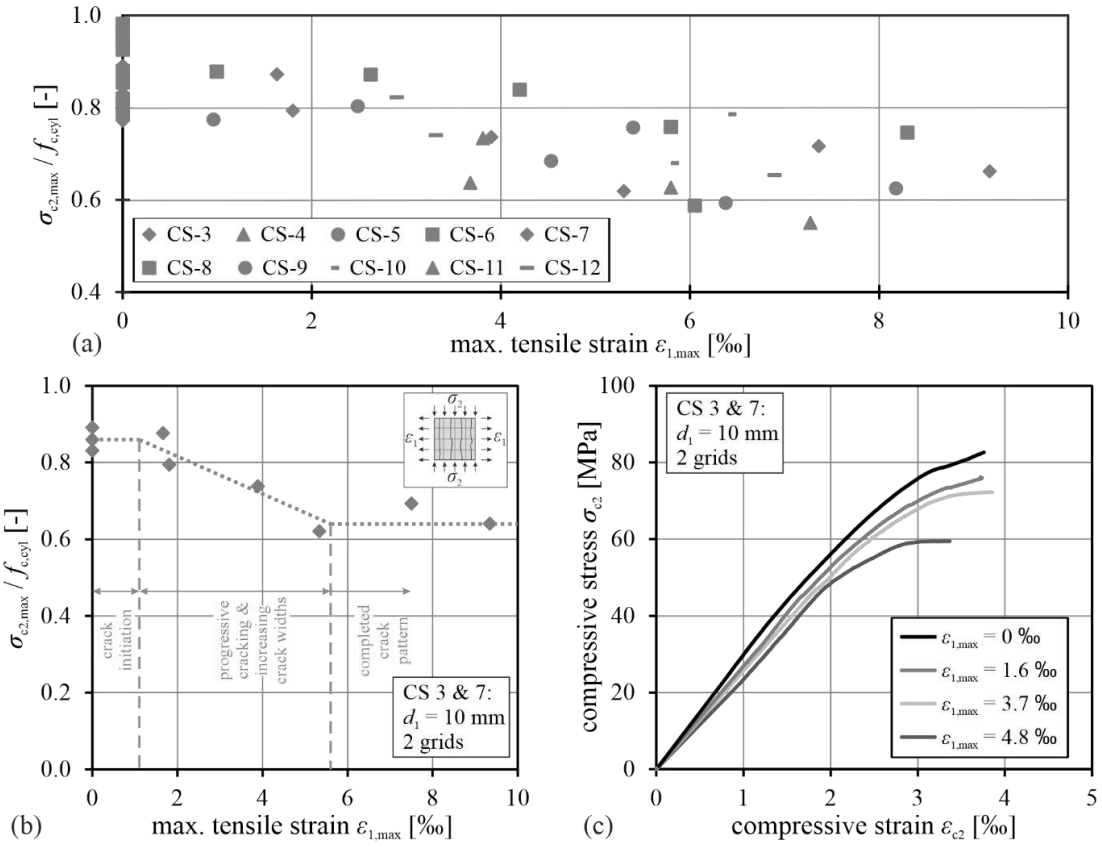

Figure 8. Influence of transverse tension on the compressive strength for all tested specimen (a) and for specimens from series 7 (b) and stress-strain curves for different max. tensile strains of specimens from series 7 (c).

In general, three cracking stages can be identified within the tests performed, depending on the average transverse tensile strain (measured with DIC), as shown for example in Figure 8 (b) for test series 7 with two grids and d_1 = 10 mm. The results show that there is no change in compressive strength until the initiation of transverse cracking. Progressive cracking then occurs, resulting in the development of smaller concrete lamellae and thus reduced compressive strength. A lower limit of strength reduction can be identified after the formation of a complete crack pattern. Similar results were found by [31] and [61] for steel reinforced panels.

Figure 8 (c) shows the influence of transverse tension on the stress-strain diagrams of reinforced specimens from series 7. For comparison, the results of one test from series 3 without transverse loading are also shown. The strains were calculated using the vertical LVDTs. The effect of compression softening can be found in the CRC specimens analogously to steel reinforced concrete. Besides the reduced compressive strength, the stiffness is also reduced with increasing transverse tension, illustrating a softer deformation response of cracked CRC.

It can thus be generally stated that the effect of compression softening also exists in CFRP-reinforced concrete and that it leads to a reduction of the compressive strength when exposed to simultaneous transverse tension and crack formation as well as to an overall softer compressive load-bearing behaviour of CRC structures.

Difference in tensile strain between concrete and yarn

Figure 9 (a) shows the related compressive strengths $\sigma_{c2,max}$ / $f_{c,cyl}$ obtained for series 7 for the applied maximum average panel tensile strain ε_1 as well as yarn tensile strain ε_{nm1}. Obviously, plotting the reduced values of compressive strength either over the yarn strain (black) or over average tensile strain measured at the concrete surface of the CRC panel (grey) leads to quite different constitutive relations for the compressive softening effect. Therefore, it is essential to specify how the

Preprints (www.preprints.org) | NOT PEER-REVIEWED | Posted: 13 December 2023 doi:10.20944/preprints202312.0950.v1

different strain values were obtained during testing and which measurement techniques have been employed.

The use of fibre optic sensors (FOS) allowed the elongation of the yarns to be measured continuously during the tests. Analogous to [58], the yarn strain, the crack width and the load introductions length can be evaluated from internal FOS measurements on reinforcement throughout the loading process. In addition, the DIC method allows for an in-depth evaluation of different strains measured at the surfaces of the concrete samples.

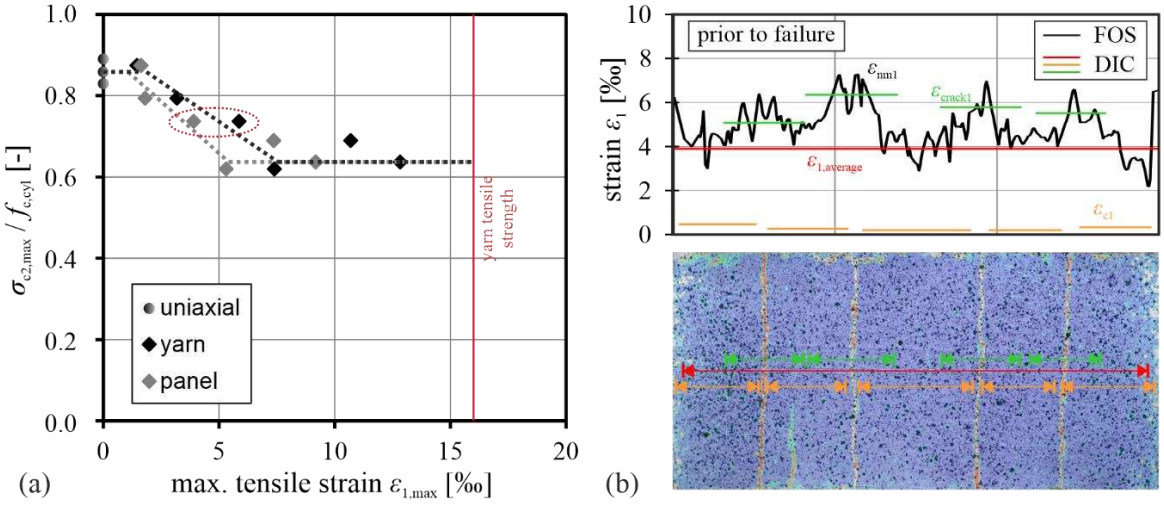

Figure 9. Relative concrete strength as a function of maximum mean panel strain and maximum yarn strain, respectively (a) and measured strains in relation to the evaluation method for specimen with two grids and d_1 = 10 mm (b).

Figure 9 (b) shows the measured strains of one specimen with two grids and d_1 = 10 mm (red circle in (a)) before compressive failure with different evaluation methods. Besides the yarn strain measured with FOS (black), the average panel strain (red), the smeared strain across a crack (green) and the concrete strain in the individual (uncracked) concrete lamellae (orange) are illustrated. The yarn strain (black) varies along the specimen's length and reaches maximum values of 7 ‰ in cracks. In addition, a smeared representation of yarn strains in the vicinity of cracks can be gained from the DIC measurements (Figure 9 (b), green). Through choosing individual measurement lengths across the cracks (according to the load introduction lengths evaluated by FOS) the yarn strain maxima measured by FOS (Figure 9 (b), black) can be well approximated by the local smeared strains across cracks (Figure 9 (b), green). The transverse tensile strains measured with DIC on the surfaces of individual (uncracked) concrete lamellae are small but visible and proof the activation and contribution of concrete to tensile force transfer (tension stiffening effect of concrete). In addition, Figure 9 (b) illustrates the DIC measurement of the average tensile strain across the entire CRC specimen (red).

DIC is also used to measure the vertical concrete compressive strains. Figure 10 shows the distribution of vertical concrete strains ε_{c2} for each individual concrete lamella of one specimen from series 7 (two grids, d_1 = 10 mm, $\varepsilon_{1,max}$ = 7.4 ‰) for different compressive load stages. As can be seen, the strains are scattered within a lamella. This strain distribution is also known from steel reinforced concrete. MIYAHARA ET AL. attributed this non-uniform stress distribution between cracks in compression to the eccentricity of the resultant forces in each lamella surrounded by cracks, resulting in a lower compressive strength compared to pure uniaxial compression [61,63]. They also ascribed this eccentricity to the complex and meandering cracks resulting from the presence of coarse aggregates. For CRC with smaller aggregates sizes, much straighter cracks are formed and therefore smaller distributions of compressive strains occur.

Preprints (www.preprints.org) | NOT PEER-REVIEWED | Posted: 13 December 2023 doi:10.20944/preprints202312.0950.v1

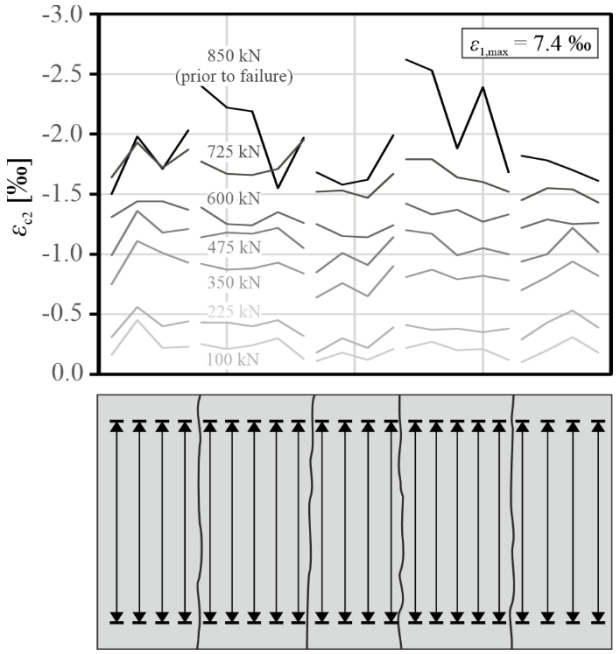

Figure 10. Compressive strain distribution during loading process for specimen with c = 10 mm, two grids and $\varepsilon_{1,max}$ = 7.4 ‰.

4.2.2. Sequential / proportional loading

In real-scale applications, different biaxial loading scenarios can occur. In CRC beams, there is usually proportional biaxial loading, because bending and shear are caused by the same external loads and thus do increase simultaneously. However, sequential loading may also occur in structural members, for example, due to restrain caused by temperature differences, resulting in a horizontal cracking. The crack widths may continue to increase or even close completely within the lifetime of the component before transverse compressive loading occurs. Therefore, two different loading scenarios were investigated in this experimental campaign. For sequential loading, the tensile load was first increased to a tensile force F_{nm} of 57 kN ($\triangleq \sigma_{nm}(t_0)$ = 1970 MPa) to induce a completed crack pattern in the specimens (Figure 11). The axial load was then increased or decreased to a predefined value and held constant while compressive loading was increased. For the proportional loading, both compressive and tensile loads were increased simultaneously with different σ_{nm1} / σ_{c2}-ratios.

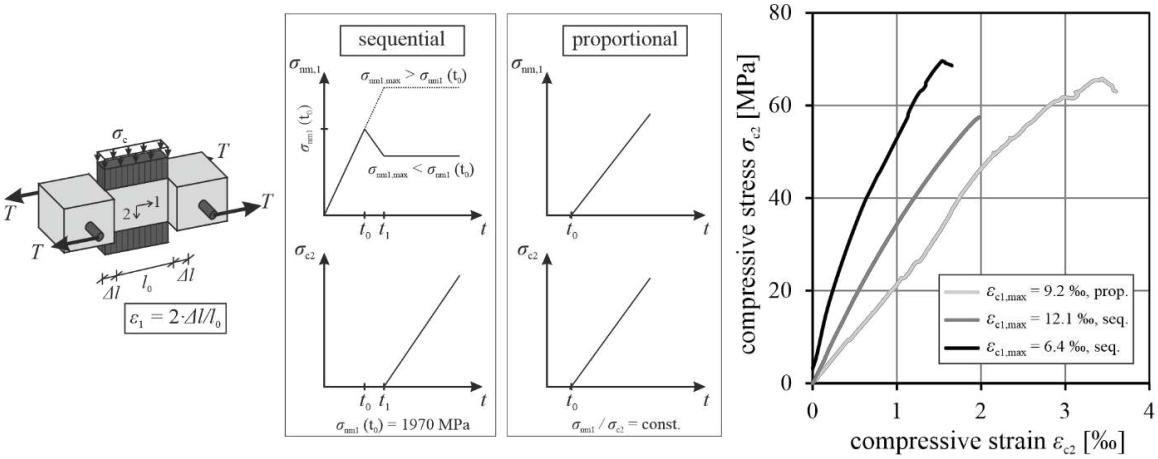

Figure 11. Influence of type of loading (sequential / proportional loading) on the compressive stress-strain behaviour.

Figure 11 shows the exemplary results of two sequentially loaded tests with different transverse tensile strains ($\varepsilon_{1,max}$ = 6.4 ‰ and $\varepsilon_{1,max}$ = 12.1 ‰) that were held constant during testing and a

Preprints (www.preprints.org) | NOT PEER-REVIEWED | Posted: 13 December 2023 doi:10.20944/preprints202312.0950.v1

proportionally loaded test in which the average tensile strain was steadily increased up to a maximum value of $\varepsilon_{1,max}$ = 9.2 ‰ at failure. Compression softening behaviour was observed for both, proportionally and sequentially loaded specimens (cf. Figure 8 (b)) and similar compressive strengths were reached for similar average tensile strains in transverse direction, confirming BETZ's [40] results for soft impregnated grids. However, despite comparable reductions in compressive strengths for both types of load application, clear differences in the stiffness and the load deformation behaviour can be observed.

Figure 11 (right) illustrates that the stress-strain behaviour of the sequential loaded specimens is generally significantly stiffer than that of the proportional loaded specimens. This can be attributed to the influence of the transverse contraction of the panel which is controlled by the Poisson's ratio of CRC. Exposed to proportional loading, the steadily increasing transverse tensile force in the CRC specimen leads to a thinning of the panel in the vertical direction caused by transverse contraction of the CRC material. This vertical strain from transverse contraction is superimposed by additional strains owing to the simultaneous acting compressive force. In consequence, we observe large total strains in vertical direction of proportionally loaded specimens caused by the superposition of compressive loading and transverse contraction.

By contrast, in tests with sequential load application, a large part of the vertical strain from transverse contraction is already generated before the actual compressive force is applied and is partially dissipated by cracking before the compression test starts. As a result, the vertical panel strains measured in the sequential compression test are generally smaller and the load-bearing behavior appears less soft than in the proportional test.

In order to cover the worst-case loading scenario, which is relevant for several full-scale applications, proportional loading was chosen for the remaining tests. In addition, the majority of tests in the literature have been performed with proportional loading, where it was also found that the type of load application had no significant effect on the compressive strength of the components.

4.2.3. Influence of concrete cover and position of CFRP grids in cross section

The influence of the lateral concrete cover and position of CFRP grids in cross section on compression softening was investigated in series CS-7 and CS-8. Table 5 summarizes the test results with proportional biaxial loading, ρ = 0.5 %, and different σ_{nm1} / σ_{c2}-ratios.

Table 5. Test results of series 7 and 8 with proportional biaxial loading and ρ = 0.5 %.

Specimen	c	$f_{c,cyl}$	F_{max}	$\sigma_{c2,max}$[1]	$\sigma_{c2,max}$ / $f_{c,cyl}$	σ_{nm1} / σ_{c2}	$\varepsilon_{1,max}$[2]
[-]	[mm]	[MPa]	[kN]	[MPa]	[-]	[-]	[%]
CS-7-1	10	93.5	891	74.2	0.79	9.9	1.6
CS-7-2	10	93.5	827	68.9	0.74	19.6	3.7
CS-7-3	10	93.5	696	58.0	0.62	29.3	4.8
CS-7-4	10	96.4	1010	84.2	0.87	3.9	1.6
CS-7-5	10	99.1	789	65.7	0.66	44.9	9.2
CS-7-6	10	99.1	853	71.1	0.72	34.6	7.4
CS-8-1	15	96.4	1016	84.7	0,88	3.9	1.0
CS-8-2	15	96.4	1009	84.1	0.87	8.7	2.6
CS-8-3	15	96.4	687	56.7	0.59	38.7	6.1
CS-8-4	15	92.9	971	78.0	0.84	17.4	3.8
CS-8-5	15	92.9	884	70.5	0.76	26.4	5.5
CS-8-6	15	92.9	884	69.3	0.75	36.1	7.7

[1]calculated using the exact dimensions of gross cross section measured with sliding gauge; [2] average panel strains evaluated using DIC.

Figure 12 (a) shows the maximum compressive strength $\sigma_{c2,max}$ standardised by $f_{c,cyl}$ of the test series 7 and 8 with different maximum average tensile strains measured on the concrete surface. For comparison, the results of the reference tests without transverse tension for d_1 = 10 mm and d_1 = 15

Preprints (www.preprints.org) | NOT PEER-REVIEWED | Posted: 13 December 2023 doi:10.20944/preprints202312.0950.v1

mm (series 3 and 4) are also shown. For the specimens with transverse tension, a reduction in the compressive strength is observed in both test series. While uniaxial compression strength is similar for both configurations, a smaller reduction in biaxial compressive strength for the same longitudinal tensile strain is found for the specimens with larger concrete cover. The behaviour can be attributed to the concentration of the reinforcement grids in the middle of the panel in series 8 (d_1 = 15 mm) leading to a deviation of compressive stress direction in only one single layer, while in series 7 (d_1 = 10 mm) the reinforcement was installed in two separate layers causing higher stress redistributions (see section 4.1). Compared to the uniaxial compression tests, the scatter was significantly reduced in the biaxial tests. Only one test with a larger concrete cover (black circle; $\varepsilon_1 \approx 6‰$) represents an outliner. This can be explained by the initial crack not being parallel to the direction of compression, resulting in premature failure. In all other specimens the cracks were parallel to the acting compressive stresses. The influence of the concrete cover or the position of the grids in the cross section, respectively, can also be seen from the stress-strain relationship of the specimens. Figure 12 (b) shows the results for specimens with almost identical transverse strains at failure but with different concrete cover. It can be seen that in addition to the larger compressive strength of the specimen with larger concrete cover (d_1 = 15 mm), the stiffness is significantly greater than that of the specimen with smaller concrete cover (d_1 = 10 mm).

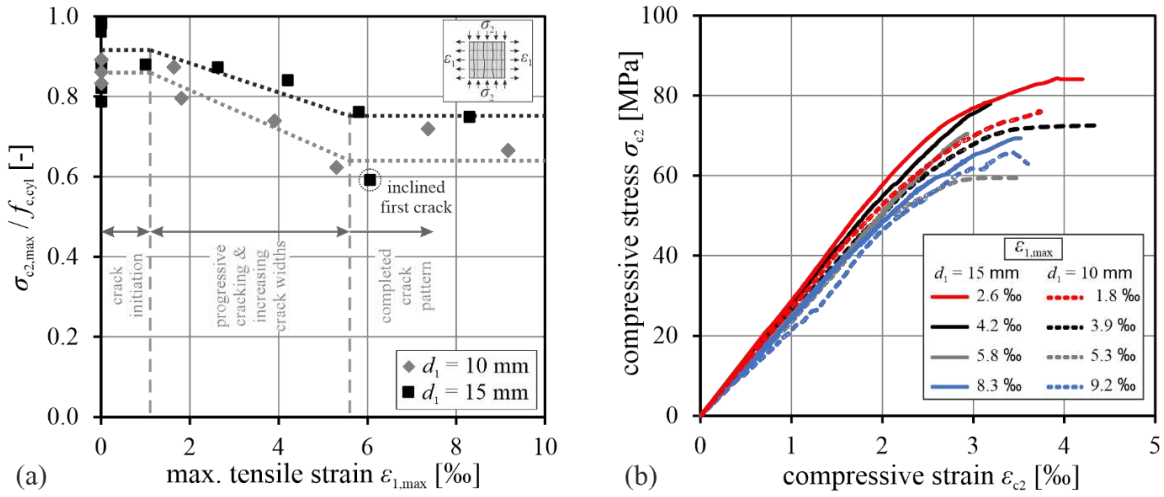

Figure 12. Compressive strength of panels for different maximum transverse tensile strains (a) and stress-strain curves of specimens with almost identical transverse strains at failure but with different concrete cover (b).

4.2.4. Influence of reinforcement ratio

To investigate the influence of the reinforcement ratio ρ, three grids were arranged in test series 9, resulting in a reinforcement ratio of 0.75 % with a constant concrete cover of 9 mm. As explained in section 4.1, no significant effect on the uniaxial compressive strength was found regardless of the increased reinforcement ratio. Figure 13 (a) shows the related compressive strengths of series 9 for different maximum tensile strains and, for comparison, the results of series 7 with two grids and the same concrete cover. Obviously, there is no reduction in compressive strength when increasing the number of grids. This phenomenon can be explained by the fact that the weakening due to the additional layer is compensated by increased longitudinal confinement of the specimen (cf. section 4.1).

Preprints (www.preprints.org) | NOT PEER-REVIEWED | Posted: 13 December 2023 doi:10.20944/preprints202312.0950.v1

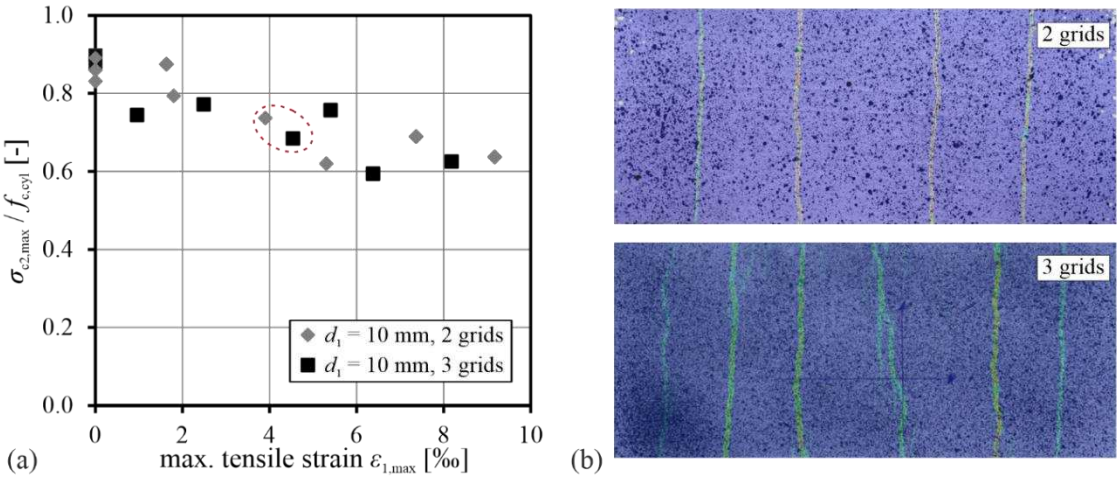

Figure 13. Influence of reinforcement ratio on compressive strength (a) and crack patterns prior to failure for specimens with similar average max. tensile strains (b).

Figure 13 (b) shows the crack patterns of two specimens with similar maximum average tensile strains in the panel. Despite only small differences in compressive strength, the crack patterns are very different. While both specimens show finely distributed cracks and therefore defined concrete struts, the specimen with three grids (bottom) has six cracks in contrast to the less reinforced specimen with four cracks (top) due to the 50 % higher reinforcement ratio. In consequence, the single crack widths are slightly reduced, while the accumulated total crack width and the average tensile strain are almost identical for both tests. Therefore, it can be concluded that the crack pattern and width of the concrete lamellae have no significant effect on the concrete compressive strength, as already stated by [61], [32], [64] for steel reinforced concrete. The reduction in strength is therefore determined by the total average transverse panel strain, independent of the number of cracks. In addition, the smaller slenderness of the individual lamellae is not critical for buckling and therefore does not affect the compressive strength.

4.2.5. Influence of skewed reinforcement

As mentioned in section 2, highly reinforced webs of CRC components often have compression strut inclinations of about 45°, while the reinforcement is aligned horizontally and vertically. Both the longitudinal and the vertical yarns induce tensile stresses in the compression strut due to bending (longitudinal yarns) and shear (vertical yarns). To investigate the influence of this skewed tensile stresses in relation to the direction of the compression strut, modified specimens were tested (test series 11 & 12). Preformed C-grids with an I-shaped cross section were used to ensure adequate anchorage of the yarns, with only the web subjected to the compressive force (Figure 4 (c)). In addition, the influence of the preformed grids was tested by also using preformed grids with 0°/90° yarn orientation, i.e., the yarns were oriented in the initial direction of the compressive and tensile load, as in the other test series. Figure 14 shows the results of these tests for different maximum tensile strains $\varepsilon_{1,max}$ (average tensile strain of the panels in the direction of tensile loading). For comparison, the test results of series 7 with planar grids and the same concrete cover are shown.

Preprints (www.preprints.org) | NOT PEER-REVIEWED | Posted: 13 December 2023 doi:10.20944/preprints202312.0950.v1

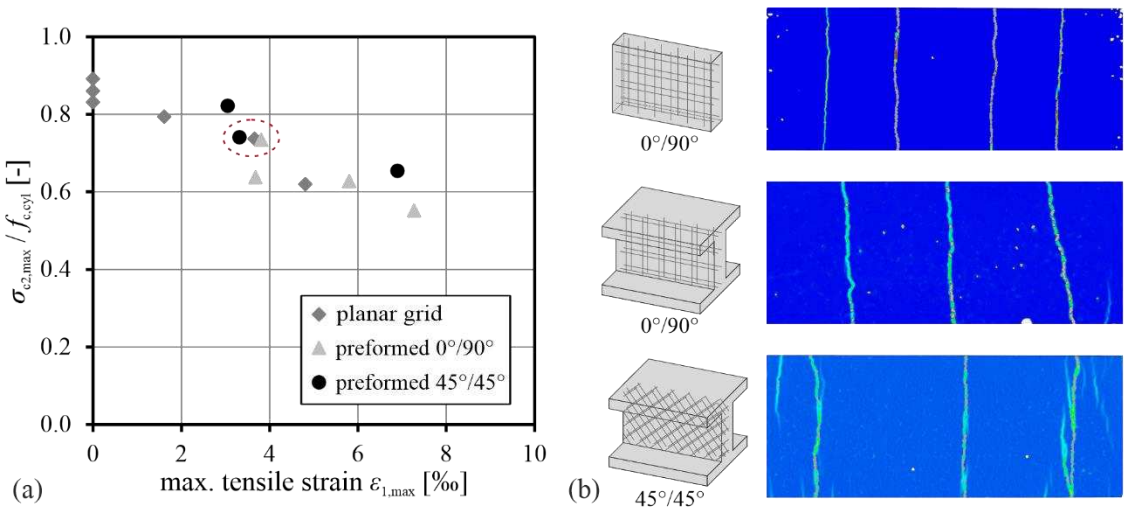

Figure 14. Influence of preformed grids and skewed reinforcement on the compression softening behaviour (b) and crack patterns of exemplary test specimens prior to failure (b).

Obviously, there is no significant influence on the strength reduction for the tests with preformed grids compared to the tests with planar grids. With regard to the influence of skewed yarns, no further reduction in compressive strength can be observed despite the tensile strain applied. This phenomenon can be explained by the emerging crack pattern (Figure 14 (b)). Due to the 45° yarn orientation, both weft and warp yarns are exposed to the same tensile stresses. Therefore, the resulting cracks are orientated parallel to the direction of compressive stresses, similar to the specimens with planar grids and thus no additional reduction in compressive strength occurs. It is also known from steel reinforced concrete that primary cracks occur perpendicularly to the principal tensile direction regardless of the orientation of the reinforcement [64]. In reinforced concrete, as the load increases, secondary cracking is often observed in the direction of the reinforcement, taking into account the reinforcement ratio in the x- and y-directions. In this instance, the primary cracks are considered as pre-damage of the component. These secondary cracks were not observed at the tensile forces applied in our tests. Both yarns had the same tensile stresses in our specimens, whereas in webs of CRC beams, different stresses may occur in the longitudinal and vertical yarns. Further tests with additional inclination angles of the grids are required to account for these differences in stress.

5. Constitutive law

Based on the results of the extensive experimental research and the measurement techniques used, a simple constitutive law is derived. It is important to note that so far only one material combination of CFRP grid and high strength concrete has been investigated and therefore the constitutive law is only valid for this combination. As explained in section 4.2.1, three sections can be identified in the relationship between maximum transverse tensile strain and compressive strength: a constant compressive strength from zero transverse strain up to the initiation of tensile cracking ①, a linear decrease in compressive strength with increasing transverse tensile strain until complete cracked state with large crack widths ②, and again a constant state for large tensile strains ③. Therefore, a three-linear approach as a function of the imposed average transverse tensile strain ($\alpha_c(\varepsilon_1)$) representing the crack states is used to describe the compression softening behaviour of CRC (Eq. (5-1)). Some parameters like the position of the grid within the cross section (number of weak layers with stress deviation) or the concrete cover, respectively, that have an effect on the maximum and minimum values of strength reduction are not covered. Here, the positive influence of concrete covers larger than 10 mm is neglected to be on the safe side and to ensure a simple calculation approach.

$$\sigma_{c2,\max} = \alpha_c(\varepsilon_1) \cdot f_{c,cyl} \tag{5-1}$$

Preprints (www.preprints.org) | NOT PEER-REVIEWED | Posted: 13 December 2023 doi:10.20944/preprints202312.0950.v1

In this constitutive law, the upper limit of compressive strength in phase ①(uncracked state and state of crack initiation) corresponds to the uniaxial compressive strength of reinforced CRC panels. Through this, splitting tensile stresses resulting from deviation of compression stresses and confinement due to CFRP grids are taken into account. For safe calculation, the mean value of the CS-3 series with the lowest mean compressive strength under uniaxial compressive load is selected. As shown in section 4.2.1, a differentiation must be made between the yarn tensile strain and the average tensile strain of the CRC panel. Analogously to common studies for steel reinforced concrete, for example [29], [65], [51], for the proposed constitutive law, α_c is derived as a function of the transverse panel strain ε_1 (Eq. (5-2)). The resulting constitutive law, as well as all test results except for tests with larger concrete cover (d_1 = 15 mm) are plotted in Figure 15. As explained in sections 4.2.4 and 4.2.5, reinforcement inclined at 45° and the reinforcement ratio (up to 0.75 %) have no significant effect on the compression softening behaviour. Therefore, these tests are included in Figure 15.

$$\alpha_c = \begin{cases} 0.86 & \text{for} \quad \varepsilon_1 \leq 1.2‰ \\ 0.92 - 0.047 \cdot \varepsilon_1 & \text{for} \quad 1.2‰ \leq \varepsilon_1 \leq 6‰ \\ 0.64 & \text{for} \quad \varepsilon_1 \geq 6‰ \end{cases} \tag{5-2}$$

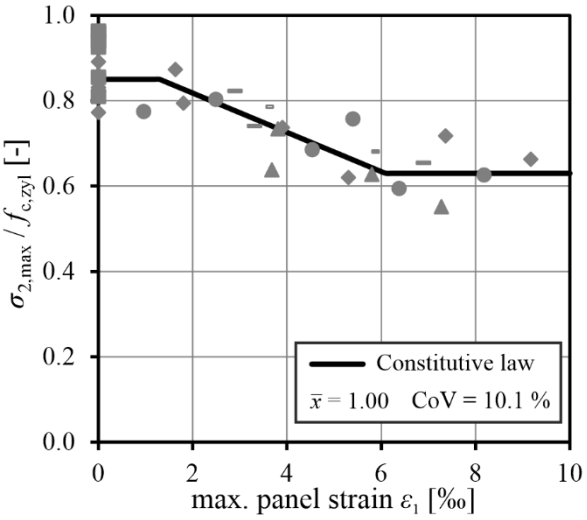

Figure 15. Description of compression softening of CRC with the material combination used as a function of panel strain.

As the load increases, more cracks develop with the crack width of the existing cracks remaining approximately constant until the entire crack pattern has developed (phase ②). When the crack pattern is completed and the average tensile strain grows beyond a certain threshold value (depending on the maximum aggregate size), stress transfer across the cracks ceases. For CRC with small aggregate sizes, this stage is reached already at small crack widths and transverse strains [66,67], so that compressive stresses are transferred within the individual lamellae. This state ③ is reached after an average tensile panel strain of about 6 ‰. This lower limit of reduction is essentially determined by the geometry of the remaining struts. The more slender, the more irregularly edged, the less they follow the direction of compression and the less constant their width, the greater the reduction in capacity of these compressive struts [51]. The high-strength concrete used, with small aggregate sizes, provides almost identical, regular lamellae, resulting in a smaller reduction in compressive strength compared to steel-reinforced concrete, which usually has larger aggregate sizes.

In general, the compression softening behaviour of the specimens tested can be described adequately with little scatter. The derived constitutive law provides a lower limit for the compressive softening behaviour of CRC panels.

6. Conclusion and outlook

CRC components provide an excellent solution for the realisation of sustainable structures with minimized use of materials. For thin-walled specimens, it is necessary to characterise the behaviour under combined compressive and transverse tensile loading, since a reduction of compressive strength occurs. Based on a literature review on the characterisation of the compression softening behaviour of steel reinforced concrete, a new test setup was developed to investigate CRC panels under uniaxial compression or biaxial compression-tension loading with refined measurement techniques. The main findings of the tests can be summarised as follows:

- In contrast to the biaxial loading test setups reported in literature, brush bearing platens were used to apply the compressive load, resulting in a reduced uniaxial compressive strength compared to panels loaded with conventional steel plates, and a significantly different fracture pattern due to the reduced lateral restraint.
- The presence of the CFRP reinforcements, which are sensitive to lateral pressure and have reduced transverse Young's modulus compared to concrete, resulted in a reduction of uniaxial compressive strength.
- The reduction in compressive strength of the fine-grained CRC panels is mainly influenced by the crack state. For uncracked reinforced concrete, no additional reduction was observed except that due to the loading conditions (rigid plates / brush bearing platens) and the presence of the yarns. Instead, for progressive cracking, a larger reduction in strength was observed at higher average transverse tensile strains in the concrete until complete cracking occurred and no further reduction in compressive strength resulted. Similar behaviour as a function of the cracking state was also observed by FEHLING ET AL. [51] for steel reinforced concrete.
- The described compression softening behaviour was also observed in the stress-strain diagrams of the specimens under biaxial loading. Higher average transverse tensile stresses result in softer compressive stiffness and lower compressive strength.
- In general, the effect of compression softening was found to be less severe in CRC compared to steel reinforced concrete.
- The compression softening behaviour strongly depends on the position of the CFRP grids within the concrete cross section. Configurations that lead to minimal deviation of concrete stresses around the weaker CFRP grids lead to stiffer compressive behaviour and higher compressive strengths. At the same time, a higher reinforcement ratio may lead to better confinement of the specimen which is also beneficial for compressive strength.
- In the tests with yarns oriented at 45° to the direction of the compressive force, both yarns showed the same strains in the warp and weft directions of the mesh. The tests did not show any additional reduction due to the orientation of the cracks parallel to the direction of the compressive forces, as in the tests with yarns oriented in the direction of the forces. These crack inclinations have also been found in slender beams tested by other researchers (e.g., [39]). However, the influence of other crack inclinations and different strains in the warp and weft yarns require further investigation.
- The compression softening behaviour can be described by a three-branched constitutive law as a function of the transverse tensile panel strain ε_{CRC1} applied with a lower limit of $0.64 \cdot f_{c,cyl}$.

The compressive softening of uniaxially cracked CRC has been extensively characterised in the present test campaign and allows the effects to be well reproduced in prismatic girder webs with parallel inclined shear cracks. However, complex shaped CRC membrane structures are usually not subjected to a single load case that causes a uniaxial crack pattern during their lifetime but experience a multitude of different loading scenarios with different load locations and intensities, resulting in biaxial or even multi-axial crack patterns. Compression softening in biaxially cracked CRC membranes and the capability of concrete struts to bridge existing cracks have not been investigated in CRC and need to be investigated in future.

Acknowledgements: Funded by THE DEUTSCHE FORSCHUNGSGEMEINSCHAFT (DFG, GERMAN RESEARCH FOUNDATION)–sfb/trr 280. Projekt-id: 417002380. The authors would like to thank the DFG for supporting the research project.

References

1. Hawkins W, Orr J, Shepherd P, Ibell T. Design, Construction and Testing of a Low Carbon Thin-Shell Concrete Flooring System. Structures 2019;18:60–71. https://doi.org/10.1016/j.istruc.2018.10.006.
2. Hegger J, Curbach M, Stark A, Wilhelm S, Farwig K. Innovative design concepts: Application of textile reinforced concrete to shell structures. Structural Concrete 2018;19(3):637–46. https://doi.org/10.1002/suco.201700157.
3. Heid A-C von der, Bosbach S, Hegger J. Production and Performance of Sandwich Elements with Textile Reinforced Facings Prestressed with CFRP. In: Zhao B, Lu X, editors. Concrete Structures for Resilient Society: Proceedings of the fib Symposium 2020; 2020, p. 280–287.
4. Kromoser B, Preinstorfer P, Kollegger J. Building lightweight structures with carbon-fiber-reinforced polymer-reinforced ultra-high-performance concrete: Research approach, construction materials, and conceptual design of three building components. Structural Concrete 2019;20(2):730–44. https://doi.org/10.1002/suco.201700225.
5. Scheerer S, Chudoba R, Garibaldi MP, Curbach M. Shells Made of Textile Reinforced Concrete - Applications in Germany. Journal IASS 2017;58(1):79–93. https://doi.org/10.20898/j.iass.2017.191.846.
6. Scholzen A, Chudoba R, Hegger J. Thin-walled shell structures made of textile-reinforced concrete: Part I: Structural design and construction. Structural Concrete 2015;16(1):106–14. https://doi.org/10.1002/suco.201300071.
7. Sharei E, Scholzen A, Hegger J, Chudoba R. Structural behavior of a lightweight, textile-reinforced concrete barrel vault shell. Composite Structures 2017;171:505–14. https://doi.org/10.1016/j.compstruct.2017.03.069.
8. Spartali H, van der Woerd JD, Hegger J, Chudoba R. Stress redistribution capacity of textile-reinforced concrete shells folded utilizing parameterized waterbomb patterns. In: IASS 2022, p. 96–106.
9. Stark A, Classen M, Knorrek C, Camps B, Hegger J. Sandwich panels with folded plate and doubly curved UHPFRC facings. Structural Concrete 2018;19(6):1851–61. https://doi.org/10.1002/suco.201700288.
10. Woerd JD van der, Bonfig C, Chudoba R, Hegger J. Construction of a vault using folded segments made out of textile reinforced concrete by fold-in-fresh. In: Bögle A, Grohmann M, editors. Interfaces: architecture.engineering.science: Proceedings of the IASS Annual Symposium 2017; 2017.
11. Beckmann B, Bielak J, Bosbach S, Scheerer S, Schmidt C, Hegger J et al. Collaborative research on carbon reinforced concrete structures in the CRC / TRR 280 project. Civil Engineering Design 2021;3(3):99–109. https://doi.org/10.1002/cend.202100017.
12. Kupfer H. Das Verhalten des Betons unter mehrachsiger Kurzzeitbelastung unter besonderer Berueckichtigung der zweiachsigen Beanspruchung. In: Deutscher Ausschuss für Stahlbeton, editor. DAfStb-Heft 229. Beuth; 1973, p. 1–95.
13. Curbach M, Scheerer S, Speck K, Hampel T. Experimentelle Analyse des Tragverhaltens von Hochleistungsbeton unter mehraxialer Beanspruchung: DAfStb-Heft 578. DAfStb: Beuth; 2011.
14. Stark A, Classen M, Hegger J. Bond behaviour of CFRP tendons in UHPFRC. Engineering Structures 2019;178:148–61. https://doi.org/10.1016/j.engstruct.2018.10.002.
15. Molter M. Zum Tragverhalten von textilbewehrtem Beton [Dissertation]. Aachen: RWTH Aachen University; 2005.
16. Voss S. Ingenieurmodelle zum Tragverhalten von textilbewehrtem Beton [Dissertation]. Aachen: RWTH Aachen University; 2008.
17. Bielak J. Shear in slabs with non-metallic reinforcement [Dissertation]. Aachen: RWTH Aachen University; 2021.
18. Bochmann J. Carbonbeton unter einaxialer Druckbeanspruchung [Dissertation]. Dresden: TU Dresden; 2019.
19. Bochmann J, Curbach M, Jesse F. Influence of artificial discontinuities in concrete under compression load-A literature review. Struct Concrete 2018;19(2):559–67. https://doi.org/10.1002/suco.201700041.
20. Reichenbach S, Preinstorfer P, Hammerl M, Kromoser B. A review on embedded fibre-reinforced polymer reinforcement in structural concrete in Europe. Construction and Building Materials 2021;307:124946. https://doi.org/10.1016/j.conbuildmat.2021.124946.
21. Brameshuber W (ed.). State-of-the-Art report of RILEM Technical Committee TC 201-TRC 'Textile Reinforced Concrete'. Bagneux: RILEM Publ; 2006.
22. Bielak J, Hegger J. Schalentragwerke aus Spritzbeton mit textiler Bewehrung: aktuelle Entwicklungen bei Bemessungs-, Herstell- und Prüfmethodik. In: Kusterle W, editor. Proceedings der Spritzbeton Tage 2018; 2018.
23. Moccia F, Yu Q, Fernández Ruiz M, Muttoni A. Concrete compressive strength: From material characterization to a structural value. Struct Concrete 2021;22(S1):634–54. https://doi.org/10.1002/suco.202000211.
24. Betz P. Carbonbeton unter Druck - Einfluss von Querdruck und Querzug. In: Deutscher Ausschuss für Stahlbeton, editor. 61. Forschungskolloquium des Deutschen Ausschusses für Stahlbeton; 2022, p. 169–174.

25. Feng D-C, Wu G, Lu Y. Finite element modelling approach for precast reinforced concrete beam-to-column connections under cyclic loading. Engineering Structures 2018;174:49–66. https://doi.org/10.1016/j.engstruct.2018.07.055.
26. Belarbi A, Hsu TTC. Constitutive laws of reinforced concrete in biaxial tension-compression. Houston, Texas; 1991.
27. Bhide SB, Collins MP. Influence of Axial Tension on the Shear Capacity of Reinforced Concrete Members. ACI SJ 1989;86(5):570–81.
28. Gehri N, Mata-Falcón J, Kaufmann W. Refined extraction of crack characteristics in large-scale concrete experiments based on digital image correlation. Engineering Structures 2022;251:113486. https://doi.org/10.1016/j.engstruct.2021.113486.
29. Vecchio F, Collins MP. The response of reinforced concrete to in-plane shear and normal stresses. Toronto, Ontario, Canada: University of Toronto, Dept. of Civil Engineering; 1982.
30. Eibl J, Neuroth U. Untersuchungen zur Druckfestigkeit von bewehrtem Beton bei gleichzeitig wirkendem Querzug; 1988.
31. Fehling E, Leutbecher T, Röder F-K, Stürwald S. Structural behavior of UHPC under biaxial loading. In: Fehling E, Schmidt M, Stürwald S, editors. Ultra High Performance Concrete (UHPC) Proceedings of the Second International Symposium on Ultra High Performance Concrete Kassel; 2008, p. 569–576.
32. Kollegger J, Mehlhorn G. Experimentelle Untersuchungen zur Bestimmung der Druckfestigkeit des gerissenen Stahlbetons bei einer Querzugbeanspruchung: DAfStb-Heft 413. Berlin: Beuth; 1990.
33. Robinson JR, Demorieux J-M. Essais de traction-compression sur modeles d'ame de poutre en béton armé [Bericht]; 1968.
34. Schlaich J, Schäfer K. Zur Druck-Querzug-Festigkeit des Stahlbetons. BuSt 1983;78(3):73–8. https://doi.org/10.1002/best.198300120.
35. Bosbach S, Bielak J, Schmidt C, Hegger J, Classen M. Influence of Transverse Tension on the Compressive Strength of Carbon Reinforced Concrete. In: Cardoso DCT, Harries KA, editors. Proceedings of 11th International Conference on Fiber-Reinforced Polymer (FRP) Composites in Civil Engineering (CICE 2023); 2023.
36. CEN/TC 250/SC 2/WG 1. prEN 1992-1-1/2021-09: Eurocode 2: Design of Concrete Structures - Part 1-1: General rules for buildings, bridges and civil engineering structures. stable version by Project Team SC2.T1; 2021.
37. Hegger J, Voss S. Textile reinforced concrete under biaxial loading. In: Prisco M Di, Felicetti R, Plizzari GA, editors. Proceedings of 6th RILEM Symposium on Fibre-Reinforced Concretes (FRC). Bagneux, France: Rilem publications; 2004, p. 1463–1472.
38. Zomorodian M. Behaviour of FRP strengthened concrete panel elements subjected to pure shear [Dissertation]. Houston, Texas: University of Houston; 2015.
39. Bielak J, Schmidt M, Hegger J, Jesse F. Structural Behavior of Large-Scale I-Beams with Combined Textile and CFRP Reinforcement. Applied Sciences 2020;10(13). https://doi.org/10.3390/app10134625.
40. Betz P, Marx S, Curbach M. Einfluss von Querzugspannungen auf die Druckfestigkeit von Carbonbeton. Beton und Stahlbetonbau 2023;118(7):524–33. https://doi.org/10.1002/best.202300028.
41. Schneider K, Butler M, Mechtcherine V. Carbon Concrete Composites C3 - Nachhaltige Bindemittel und Betone für die Zukunft. BuSt 2017;112(12):784–94. https://doi.org/10.1002/best.201700058.
42. Bielak J, Schöneberg J, Classen M, Hegger J. Shear capacity of continuous concrete slabs with CFRP reinforcement. Construction and Building Materials 2022;320. https://doi.org/10.1016/j.conbuildmat.2021.126117.
43. Bielak J. On the role of dowel action in shear transfer of CFRP textile-reinforced concrete slabs. Composite Structures 2023;311:116812. https://doi.org/10.1016/j.compstruct.2023.116812.
44. Deutsches Institut für Normung e.V. Prüfung von Festbeton- Teil 3: Druckfestigkeit von Probekörpern: Deutsche Fassung EN 12390-3:2019;91.100.30(DIN EN 12390-3:2019-10). Berlin: Beuth; 2019. https://doi.org/10.31030/3045735.
45. Deutsches Institut für Normung e.V. Prüfung von Festbeton – Teil 13: Bestimmung des Elastizitätsmoduls unter Druckbelastung (Sekantenmodul): Deutsche Fassung EN 12390-13:2021;91.100.30(DIN EN 12390-13:2021-09). Berlin: Beuth; 2021.
46. Deutsches Institut für Normung e.V. Prüfverfahren für Zement - Teil 1: Bestimmung der Festigkeit: Deutsche Fassung EN 196-1:2016;91.100.10(DIN EN 196-1:2016-11). Berlin: Beuth; 2016.
47. Deutscher Ausschuss für Stahlbeton. DAfStb-Richtlinie Betonbauteile mit nichtmetallischer Bewehrung - Entwurf vom 06. September 2022: D194. Berlin: Beuth; 2022.
48. Bosbach S, Hegger J, Classen M. Dowel action of textile CFRP shear reinforcement in carbon reinforced concrete. Construction and Building Materials 2023(under review).
49. Bergmann S, Classen M, Hegger J. Experimental study on the shear behavior of multi-span CFRP reinforced beams with shear reinforcement subjected to concentrated and distributed loading. Buildings 2023 (under review).

50. Schütze E, Bielak J, Scheerer S, Hegger J, Curbach M. Einaxialer Zugversuch für Carbonbeton mit textiler Bewehrung. BuSt 2018;113(1):33–47. https://doi.org/10.1002/best.201700074.
51. Fehling E, Leutbecher T, Röder F-K. Zur Druck-Zug-Festigkeit von Stahlbeton und stahlfaserverstärktem Stahlbeton. BuSt 2009;104(8):471–84. https://doi.org/10.1002/best.200900020.
52. Becks H, Bielak J, Hegger J. Interaction of normal and shear loads in carbon reinforced slab segments. In: IABSE, editor. Proceedings of IABSE Congress: Structural Engineering for Future Societal Needs; 2021, p. 1233–1241.
53. Kupfer H, Hilsdorf HK, Ruesch H. Behavior of Concrete Under Biaxial Stresses. ACI Journal 1969:656 bis 666.
54. Gerstle KH, Aschl H, Bellotti R, Beracchi P, Kotsovos MD, Ko H-Y et al. Behaviour of Concrete under Multiaxial Stress States. Journal of the Engineering Mechanics Division 1980;Vol. 106(No. EM6).
55. Deutsches Institut für Normung e.V. Prüfung von Festbeton - Teil 1: Form, Maße und andere Anforderungen für Probekörper und Formen: Deutsche Fassung EN 12390-1:2012;91.100.30(DIN EN 12390-1:2012-12). Berlin: Beuth; 2012.
56. Bielak J, Spelter A, Will N, Claßen M. Verankerungsverhalten textiler Bewehrungen in dünnen Betonbauteilen. BuSt 2018;113(7):515–24. https://doi.org/10.1002/best.201800013.
57. Becks H, Baktheer A, Marx S, Classen M, Hegger J, Chudoba R. Monitoring concept for the propagation of compressive fatigue in externally prestressed concrete beams using digital image correlation and fiber optic sensors. Fatigue & Fracture of Engineering Materials & Structures 2023;46(2):514–26. https://doi.org/10.1111/ffe.13881.
58. Becks H, Bielak J, Camps B, Hegger J. Application of fiber optic measurement in textile-reinforced concrete testing. Struct Concrete 2021. https://doi.org/10.1002/suco.202100252.
59. Janiak T, Becks H, Camps BH, Hegger J. A unified approach to the evaluation of distributed fibre optic sensors in structural concrete. Materials and Structures 2023(accepted).
60. European Standard. Eurocode 2: Design of concrete structures – Part 1-1: General rules and rules for buildings. Incl. Corrigendum 1: EN 1992-1-1:2004/AC:2008, incl. Corrigendum 2: EN 1992-1-1:2004/AC:2010, incl. Amendment 1: EN 1992-1-1:2004/A1:2014(EN 1992-1-1:2004/A1); 2014.
61. Miyahara T, Kawakami T, Maekawa K. Nonlineat behavior of cracked reinforced concrete plate element. Concrete Library of JSCE 1988(11).
62. Schießl A. Die Druckfestigkeit von gerissenen Scheiben aus Hochleistungsbeton und selbstverdichtendem Beton unter besonderer Berücksichtigung des Einflusses der Rissneigung. Deutscher Ausschuss für Stahlbeton 2005(548).
63. Maekawa K. The deformational behavior and constitutive equation of concrete based on the elasto-plastic and fracture model [Dissertation]. Tokyo: University of Tokyo; 1985.
64. Roos W. Zur Druckfestigkeit des gerissenen Stahlbetons in scheibenförmigen Bauteilen bei gleichzeitig wirkender Querzugbelastung [Dissertation]. München: Technische Universität München; 1995.
65. Kaufmann W, Marti P. Structural Concrete: Cracked Membrane Model. J. Struct. Eng. 1998;124(12):1467–75. https://doi.org/10.1061/(ASCE)0733-9445(1998)124:12(1467).
66. Classen M, Hegger J. Shear Tests on Composite Dowel Rib Connectors in Cracked Concrete. ACI SJ 2018;115(3). https://doi.org/10.14359/51701295.
67. Ungermann J, Adam V, Classen M. Fictitious Rough Crack Model (FRCM): A Smeared Crack Modelling Approach to Account for Aggregate Interlock and Mixed Mode Fracture of Plain Concrete. Materials 2020;13(12):2774. https://doi.org/10.3390/ma13122774.